INTERNATIONAL JOURNAL FOR NUMERICAL METHODS IN FLUIDS, VOL. 19, 513–525 (1994)

FINITE ELEMENT SOLUTION OF THE STREAMFUNCTION–VORTICITY EQUATIONS FOR INCOMPRESSIBLE TWO-DIMENSIONAL FLOWS

G. COMINI, M. MANZAN AND C. NONINO

Istituto di Fisica Tecnica e di Tecnologie Industriali, Università degli Studi di Udine, Viale Ungheria 43, I-33100 Udine, Italy

SUMMARY

The streamfunction–vorticity equations for incompressible two-dimensional flows are uncoupled and solved in sequence by the finite element method. The vorticity at no-slip boundaries is evaluated in the framework of the streamfunction equation. The resulting scheme achieves convergence, even for very high values of the Reynolds number, without the traditional need for upwinding. The stability and accuracy of the approach are demonstrated by the solution of two well-known benchmark problems: flow in a lid-driven cavity at $Re \leqslant 10{,}000$ and flow over a backward-facing step at $Re = 800$.

KEY WORDS Finite elements Incompressible viscous flow Streamfunction–vorticity Vorticity boundary conditions

1. INTRODUCTION

In the analysis of two-dimensional incompressible flows the streamfunction–vorticity formulation of the Navier–Stokes equations allows the elimination of pressure from the problem and automatically satisfies the continuity constraint. On the other hand, the value of the vorticity at no-slip boundaries is difficult to specify and a poor evaluation of this boundary condition leads, almost invariably, to serious difficulties in obtaining a converged solution.[1] Traditional finite element approaches based on finite difference formulae for the wall vorticity are generally limited to regular domains and to low-Reynolds-number flows. Therefore in recent years a lot of effort has been devoted to the consistent specification of the vorticity at no-slip boundaries in the context of both Galerkin and control-volume-based finite element methods.[2–9]

A guideline for a correct specification of boundary conditions at no-slip walls has been given by Roache.[1] His numerical recipe can be summarized as follows: *at no-slip walls first specify the streamfunction and then, in the procurement of the wall vorticity, utilize the additional information on the normal component of the streamfunction.* In this way the boundary conditions for the streamfunction are not overspecified and the wall vorticity is correctly related to the tangential component of the velocity. Obviously, at stationary walls the tangential component of the velocity is zero, but at moving walls serious errors may result if the gradient of the streamfunction is not properly taken into account. These ideas have been incorporated in the control-volume-based finite element method[6] and have also been utilized to develop a postprocessing formula for approximating the vorticity on the boundary in either finite element or finite difference computations.[8]

For the implementation of the no-slip boundary condition in the context of the finite element

CCC 0271–2091/94/180513–13

Received September 1993
Revised April 1994

method various approaches have been followed, ranging from fully integrated to fully segregated procedures. In Reference 2 the streamfunction, the wall vorticity and the field vorticity are computed simultaneously. In Reference 5 first the streamfunction and the wall vorticity are solved simultaneously and then the field vorticity is solved separately. In the present study we solve first the streamfunction equation, then we compute the wall vorticity as suggested in Reference 8 and finally we compute the field vorticity. In this way we generalize the results of Reference 5, following a fully segregated approach in which the two differential equations are completely uncoupled and dealt with in sequence. Moreover, in the discretization of the streamfunction equation our approach leads to smaller matrices and preserves the symmetry, which is lost in Reference 5 because of the simultaneous solution of streamfunction and wall vorticity.

In the finite element formulation we rely on the Bubnov–Galerkin method for space discretization, without using any upwinding technique. Thus we reach convergence, even for very high values of the Reynolds number, without exploiting the effects of the numerical viscosity introduced by most upwinding procedures. The stability and accuracy of our approach are demonstrated by the solution of two well-known benchmark problems: flow in a lid-driven cavity at $Re \leqslant 10{,}000$ and flow over a backward-facing step at $Re = 800$.

2. STATEMENT OF THE PROBLEM

For two-dimensional incompressible laminar flows the streamfunction and vorticity equations can be written in dimensionless form as[4,6,9]

$$\partial^2\psi/\partial x^2 + \partial^2\psi/\partial y^2 = -\omega \tag{1}$$

and

$$\frac{\partial\omega}{\partial t} + Re\left(u\frac{\partial\omega}{\partial x} + v\frac{\partial\omega}{\partial y}\right) = \frac{\partial^2\omega}{\partial x^2} + \frac{\partial^2\omega}{\partial y^2} + b \tag{2}$$

respectively. In the above equations ψ is the streamfunction, x and y are Cartesian co-ordinates,

$$u = \partial\psi/\partial y \tag{3}$$

and

$$v = -\partial\psi/\partial x \tag{4}$$

are the velocity components in the x- and y-directions respectively,

$$\omega = \partial v/\partial x - \partial u/\partial y \tag{5}$$

is the vorticity, t is the time, b is the body force and Re is the Reynolds number.

In the problems considered here we have inflow boundaries, outflow boundaries and no-slip walls that can be either stationary or moving. At inflow boundaries the velocity field is completely specified and consequently we know the tangential velocity component u_s, the normal velocity component u_n and their derivatives with respect to n and s. Thus at inflow boundaries we can compute the values of the vorticity as

$$\omega = \partial u_s/\partial n - \partial u_n/\partial s = \omega_p \tag{6}$$

and we can prescribe these values as boundary conditions of the first kind for equation (2). Furthermore, at inflow boundaries we can also prescribe the normal derivative of the streamfunction

$$\partial\psi/\partial n = -u_s \tag{7}$$

as a general boundary condition of the second kind for equation (1). Usually at inflow boundaries we have an orthogonal incoming flow with $u_s = 0$, but we can also have u_s different from zero, leading to a skew incoming flow.

At outflow boundaries we generally assume fully developed flow conditions and a zero tangential velocity, leading to the boundary condition

$$\partial\omega/\partial n = 0 \tag{8}$$

and

$$\partial\psi/\partial n = 0 \tag{9}$$

for the vorticity and streamfunction respectively.

At no-slip boundaries the value of the streamfunction is known,

$$\psi = \psi_p, \tag{10}$$

since the walls are also streamlines. On the other hand, the tangential component of the velocity must be specified too, leading to the additional boundary condition of the second kind yielded by equation (7). However, this additional condition cannot be used for the solution of the streamfunction equation because it would overspecify the problem.[1] Consequently the information on the gradient of the streamfunction must be incorporated in the boundary condition for the vorticity. Therefore at no-slip boundaries we must obtain the values of the wall vorticity from a solution of equation (1) where condition (7) is taken into account. These ideas are implemented in the finite element formulation illustrated in the next section.

3. FINITE ELEMENT FORMULATION

As usual we approximate the unknown variables throughout the solution domain by means of the standard expansions

$$\psi \approx \sum_{i=1}^{n} N_i\psi_i = \mathbf{N}\boldsymbol{\psi} \tag{11}$$

and

$$\omega \approx \sum_{i=1}^{n} N_i\omega_i = \mathbf{N}\boldsymbol{\omega}, \tag{12}$$

where N_i are shape functions, ψ_i and ω_i are nodal values of ω and ψ respectively and n is the total number of nodes in the discretization. Substituting equations (11) and (12) into equations (1) and (2) and following the Bubnov–Galerkin method, we arrive at two systems of space-discretized equations which can be written in matrix form as

$$\mathbf{K}\boldsymbol{\psi} = \mathbf{M}\boldsymbol{\omega} - \mathbf{q} \tag{13}$$

and

$$\mathbf{M}\dot{\boldsymbol{\omega}} + (\mathbf{K} + \mathbf{A})\boldsymbol{\omega} = \mathbf{s}. \tag{14}$$

In the above equations we have

$$\dot{\boldsymbol{\omega}} = \partial\boldsymbol{\omega}/\partial t \tag{15}$$

and we refer to the usual definitions of matrix and vector entries

$$K_{ij} = \int_{\Omega}\left(\frac{\partial N_i}{\partial x}\frac{\partial N_j}{\partial x} + \frac{\partial N_i}{\partial y}\frac{\partial N_j}{\partial y}\right) \mathrm{d}\Omega, \tag{16}$$

$$M_{ij} = \int_{\Omega} N_i N_j \, \mathrm{d}\Omega, \tag{17}$$

$$q_i = \int_{\Gamma} N_i u_s \, \mathrm{d}\Gamma, \tag{18}$$

$$A_{ij} = Re \int_{\Omega} N_i\left(u\frac{\partial N_j}{\partial x} + v\frac{\partial N_j}{\partial y}\right) \mathrm{d}\Omega \tag{19}$$

and

$$s_i = \int_{\Omega} N_i b \, \mathrm{d}\Omega. \tag{20}$$

In the above equations Ω is the domain, Γ is the no-slip boundary and we have $i, j = 1, \ldots, n$.

Equations (13) and (14) can be decoupled and solved in sequence, provided that special care is taken to properly represent the boundary conditions. Our calculation procedure to advance from the time step $m \geqslant 0$ to the time step $m + 1$ can be described as follows.

First, from equation (13) and the values of vorticity at the time step m we compute the new values of the streamfunction as

$$\boldsymbol{\psi}^{m+1} = \mathbf{K}^{-1}(\mathbf{M}\boldsymbol{\omega}^m - \mathbf{q}). \tag{21}$$

In the solution of the streamfunction equation the nodal values ψ_i are known at both stationary and moving walls. Thus in system (21) we eliminate the corresponding equations which are the only ones where the entries in the vector $\mathbf{q}$ can be different from zero.

Then, from equation (13) and the values of the streamfunction obtained from equation (21) we compute the values of vorticity at no-slip boundaries as

$$\boldsymbol{\omega}^{m+1} = \mathbf{M}^{-1}(\mathbf{K}\boldsymbol{\psi}^{m+1} + \mathbf{q}), \tag{22}$$

where the entries in the vector $\mathbf{q}$ are taken into account and calculated according to equation (18). Actually, in system (22) we do not even have to consider a complete new solution, since the computations involve only a strip of elements adjacent to the walls.

Finally, by estimating the velocity components at the previous time step as

$$u^m = (\partial\psi/\partial y)^m \tag{23}$$

and

$$v^m = -(\partial\psi/\partial x)^m, \tag{24}$$

we can linearize and integrate, with respect to time, equation (14). Using standard finite difference approximation for the time variable, we obtain a recursive scheme for time integration,

$$\boldsymbol{\omega}^{m+1} = \left(\frac{\mathbf{M}}{\Delta t} + \vartheta(\mathbf{K} + \mathbf{A}^m)\right)^{-1}\left[\left(\frac{\mathbf{M}}{\Delta t} - (1-\vartheta)(\mathbf{K} + \mathbf{A}^m)\right)\boldsymbol{\omega}^m + \mathbf{s}\right], \tag{25}$$

that leads to the explicit algorithm for $\vartheta = 0$, to the Crank–Nicolson algorithm for $\vartheta = \frac{1}{2}$ and to the fully implicit algorithm for $\vartheta = 1$.

Once a solution has been obtained in terms of streamfunction and vorticity, the evaluation of velocity components at the nodes can be easily obtained from the weighted residual approximations of equations (3) and (4).

4. RESULTS AND DISCUSSION

The examples presented here concern steady state solutions of two well-known benchmark problems: flow in a lid-driven cavity and flow over a backward-facing step. Since we were only interested in the stationary results obtained from pseudotransient simulations, we always used the fully implicit algorithm for time integration. In this way we were able to consistently exceed by a factor of about 10 the stability limits for explicit algorithms. As a convergence criterion we considered the difference in computed streamfunction fields and we terminated the calculation when the Euclidean norm of changes between two consecutive time steps was less than 10^{-5}. In the numerical simulations we employed only the conventional Bubnov–Galerkin formulation described in the previous section, with four-node and eight-node isoparametric elements and consistent mass matrices. The systems of algebraic equations obtained from the finite element discretizations were solved by means of iterative procedures derived from the family of preconditioned conjugate gradient (CG) and preconditioned conjugate residual (CR) methods.[10,11] We used a non-symmetric conjugate gradient squared (CGS) solver for the vorticity equation and a symmetric CR solver for the streamfunction equation. In this way we took full advantage of the symmetric, positive definite nature of the coefficient matrix of the discretized streamfunction equation resulting from our formulation.

Flow in a lid-driven square cavity

To study the dependence of the time step on the spatial spacing and to investigate the accuracy of the method, we considered first a sequence of uniformly spaced grids of linear elements consisting of 21 × 21, 31 × 31 and 41 × 41 mesh points. Instead, for the solution of the benchmark problem we used 41 × 41 grid points (40 × 40 elements) with a finer mesh subdivision near the walls. The mesh employed in the final calculations is shown in Figure 1 together with the imposed boundary conditions. The smallest dimensionless element size is 0·008 at the four corners and the largest is 0·04 at the centre of the cavity. The selected Reynolds numbers are based on the lid velocity and on the reference length given by the depth (and width) of the square cavity.

Numerous researchers have performed computations for $Re = 1000$. Thus the flow conditions defined by this Reynolds number were chosen to investigate the influence of the mesh design on our solution. The essential feature of the test problem is the prediction of locations and intensities of various vortices inside the cavity. In Table I we show for the various meshes the minimum value of the streamfunction, the corresponding location of the primary vortex centre and the time step used. As we can see, with the finer meshes the results become rather insensitive

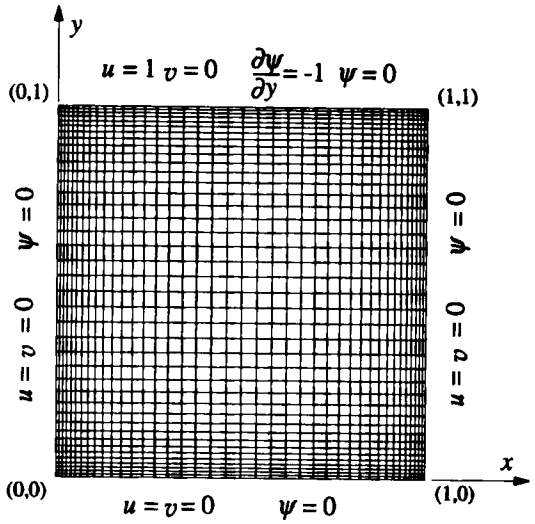

Figure 1. Finite element mesh and boundary conditions for a two-dimensional laminar flow in a lid-driven cavity

Table I. Dependence of the results and the time step on the mesh used at $Re = 1000$

Grid	Primary vortex centre			Time step
	x	y	ψ	Δt
21 × 21 regular	0·529	0·586	−0·108	0·5
31 × 31 regular	0·530	0·570	−0·117	0·4
41 × 41 regular	0·530	0·567	−0·119	0·25
41 × 41 stretched	0·531	0·565	−0·119	0·02

to the subdivision of the domain, while the time step depends on the dimension of the smallest elements and must be reduced even if the mesh is only stretched.

As we have already pointed out, we used a fully implicit time integration algorithm to obtain the steady state (converged) solutions. Thus an essential question of this study is the long-term behaviour of the solution fields. A good indication of whether or not the governing equations are converging is given by the behaviour of the Euclidean norm of the residuals. The residuals at the time step m can be defined as

$$\mathbf{r}_m^{\omega} = \mathbf{M}\dot{\boldsymbol{\omega}} = \mathbf{s} - (\mathbf{K} + \mathbf{A}^m)\boldsymbol{\omega}^m \tag{26}$$

and

$$\mathbf{r}_m^{\psi} = (\mathbf{M}\boldsymbol{\omega}^m - \mathbf{q}) - \mathbf{K}\boldsymbol{\psi}^m \tag{27}$$

for the vorticity and streamfunction equations respectively. Thus a convergence criterion can be easily established by considering the relative residuals

$$r_r^{\omega} = \|\mathbf{r}_m^{\omega}\|_2 / \|\mathbf{r}_0^{\omega}\|_2 \tag{28}$$

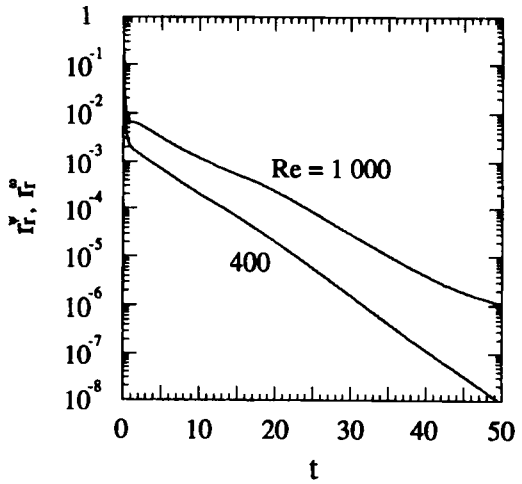

Figure 2. Normalized residuals for the lid-driven cavity flow. For the same Reynolds number the normalized residuals of the vorticity and streamfunction are practically indistinguishable

and

$$r_r^{\psi} = \|\mathbf{r}_m^{\psi}\|_2 / \|\mathbf{r}_0^{\psi}\|_2 \tag{29}$$

defined as ratios of the Euclidean norm of the current residual to the Euclidean norm of the initial residual. In Figure 2 we plot the normalized residuals of the vorticity and streamfunction for the different values of the Reynolds number with reference to the subdivision of the domain illustrated in Figure 1. The plot demonstrates the clear tendency of our algorithm towards convergence and shows that the normalized residuals of the vorticity and streamfunction pertaining to the same Reynolds number are practically indistinguishable. The Euclidean norm of changes in the streamfunction between two consecutive steps behaves like the residuals. Therefore in our applications we could confidently choose a convergence criterion based on this norm.

The flow conditions investigated in the final calculations concern the Reynolds numbers 400, 1000, 5000 and 10,000. For $Re = 400$ and 1000 we started from uniform initial conditions $\psi = \omega = 0$, while for higher values of the Reynolds number we used as initial conditions the steady state solution corresponding to a lower Reynolds number. The time steps employed were $\Delta t = 0{\cdot}01$ for $Re = 400$ and $\Delta t = 0{\cdot}02$ for all other flow conditions. The number of time steps required to reach convergence ranged from a minimum of about 1100 for $Re = 400$, starting from uniform initial conditions, to a maximum of about 2400 for $Re = 10{,}000$, starting from the stationary flow conditions at $Re = 5000$.

The streamfunction contours are shown in Figure 3 and the values of ψ along the contours are listed in Table II. These results compare very favourably with some of the most reliable data reported in the literature,[12–15] even though we used a lower number of nodal points. In fact, Ghia *et al.*[12] used 129 × 129 mesh points for $Re \leqslant 3200$ and 257 × 257 mesh points for $Re \geqslant 5000$, Sohn[14] used 40 × 40 nine-node elements (81 × 81 grid points), while Gresho *et al.*[13] and Tanahashi *et al.*[15] used 50 × 50 linear elements (51 × 51 grid points). In Figure 4 we compare our predictions of the velocity profiles through the centre of the cavity with those of Ghia *et al.*,[12] demonstrating excellent agreement for all Reynolds numbers. Finally, to obtain some more quantitative comparisons with the results of References 12–14, in Table III we report the extreme

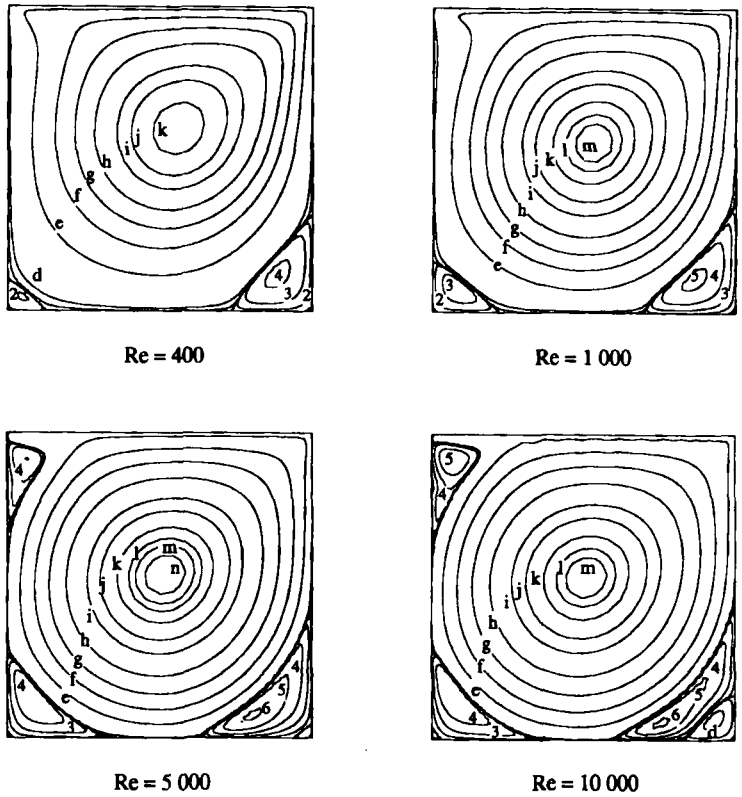

Figure 3. Streamfunction contours in a lid-driven cavity for different Reynolds numbers (contour values are reported in Table II)

Table II. Values of streamline contours in Figure 3

Contour letter	Streamfunction ψ	Contour letter	Streamfunction ψ	Contour number	Streamfunction ψ
a	$-1{\cdot}0 \times 10^{-10}$	h	$-0{\cdot}0700$	1	$1{\cdot}0 \times 10^{-7}$
b	$-1{\cdot}0 \times 10^{-7}$	i	$-0{\cdot}0900$	2	$1{\cdot}0 \times 10^{-5}$
c	$-1{\cdot}0 \times 10^{-5}$	j	$-0{\cdot}1000$	3	$1{\cdot}0 \times 10^{-4}$
d	$-1{\cdot}0 \times 10^{-4}$	k	$-0{\cdot}1100$	4	$5{\cdot}0 \times 10^{-4}$
e	$-0{\cdot}0100$	l	$-0{\cdot}1150$	5	$1{\cdot}5 \times 10^{-3}$
f	$-0{\cdot}0300$	m	$-0{\cdot}1175$	6	$3{\cdot}0 \times 10^{-3}$
g	$-0{\cdot}0500$	n	$-0{\cdot}1200$		

values of the streamfunction. On average our values are in better agreement with the results of Ghia *et al.*[12] than most published finite element results.

Flow over a backward-facing step

The geometry and boundary conditions defining the test problem are shown in Figure 5 (a), while the mesh employed in the numerical simulations is shown in Figure 5 (b). The aspect ratio of the step to the channel height is 1:2, giving a step height equal to one-half of the channel

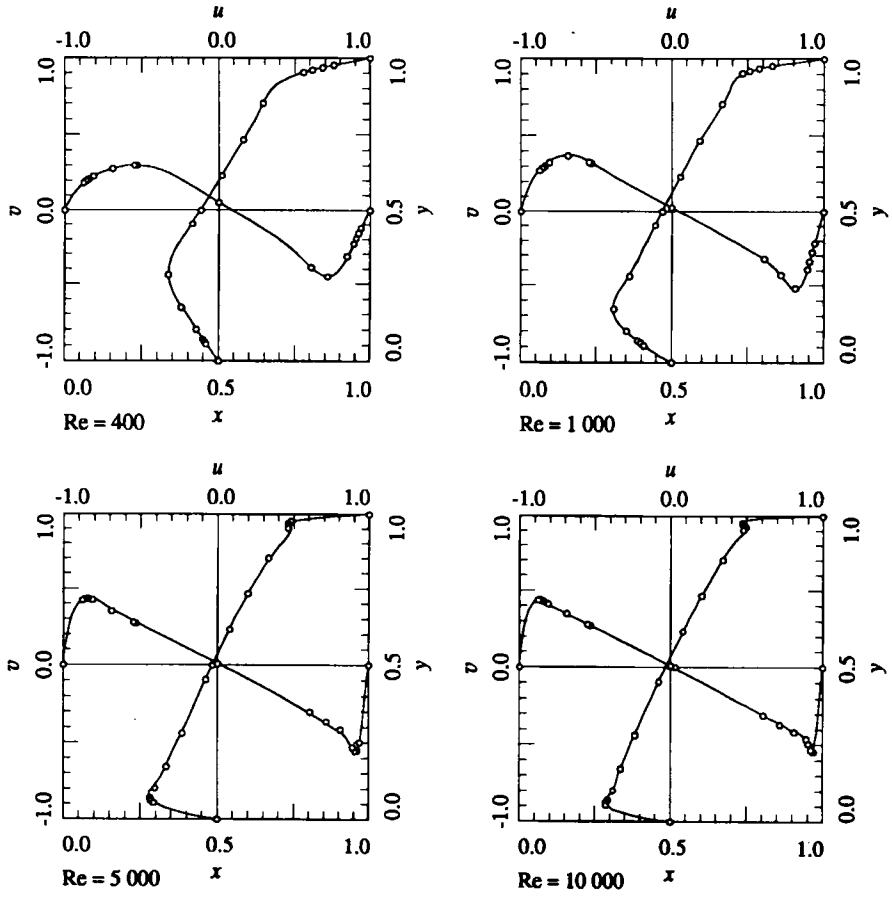

Figure 4. Velocity profiles through the centre of a lid-driven cavity for different Reynolds numbers (—, present work; ○, Reference 12)

Table III. Extreme values of streamfunctions at various vortices inside a lid-driven cavity

Re	Primary vortex	Top left	Bottom left 1	Bottom left 2	Bottom right 1	Bottom right 2	Reference
400	−0·114		$1{\cdot}23 \times 10^{-5}$		$6{\cdot}38 \times 10^{-4}$	$-2{\cdot}02 \times 10^{-8}$	Present work
	−0·114		$1{\cdot}42 \times 10^{-5}$	$-7{\cdot}67 \times 10^{-10}$	$6{\cdot}42 \times 10^{-4}$	$-1{\cdot}87 \times 10^{-8}$	Ghia *et al.*[12]
	−0·112		$1{\cdot}32 \times 10^{-5}$		$6{\cdot}13 \times 10^{-4}$	$-1{\cdot}63 \times 10^{-8}$	Sohn[14]
1000	−0·119		$2{\cdot}41 \times 10^{-4}$		$1{\cdot}76 \times 10^{-3}$	$-6{\cdot}05 \times 10^{-8}$	Present work
	−0·118		$2{\cdot}31 \times 10^{-4}$	$-1{\cdot}14 \times 10^{-9}$	$1{\cdot}75 \times 10^{-3}$	$-9{\cdot}32 \times 10^{-8}$	Ghia *et al.*[12]
	−0·114		$2{\cdot}00 \times 10^{-4}$		$1{\cdot}76 \times 10^{-3}$	$-1{\cdot}80 \times 10^{-8}$	Gresho *et al.*[13]
	−0·115		$2{\cdot}17 \times 10^{-4}$		$1{\cdot}63 \times 10^{-3}$	$-1{\cdot}20 \times 10^{-8}$	Sohn[14]
5000	−0·122	$1{\cdot}53 \times 10^{-3}$	$1{\cdot}37 \times 10^{-3}$	$-7{\cdot}83 \times 10^{-8}$	$3{\cdot}25 \times 10^{-3}$	$-1{\cdot}97 \times 10^{-6}$	Present work
	−0·119	$1{\cdot}46 \times 10^{-3}$	$1{\cdot}36 \times 10^{-3}$	$-7{\cdot}09 \times 10^{-8}$	$3{\cdot}08 \times 10^{-3}$	$-1{\cdot}43 \times 10^{-6}$	Ghia *et al.*[12]
	−0·109	$1{\cdot}23 \times 10^{-3}$	$1{\cdot}49 \times 10^{-3}$	$-2{\cdot}85 \times 10^{-8}$	$3{\cdot}87 \times 10^{-3}$	$-5{\cdot}22 \times 10^{-8}$	Gresho *et al.*[13]
	−0·115	$1{\cdot}28 \times 10^{-3}$	$1{\cdot}25 \times 10^{-3}$	$-4{\cdot}93 \times 10^{-8}$	$2{\cdot}80 \times 10^{-3}$	$-7{\cdot}12 \times 10^{-7}$	Sohn[14]
10000	−0·120	$2{\cdot}57 \times 10^{-3}$	$1{\cdot}44 \times 10^{-3}$	$-4{\cdot}48 \times 10^{-7}$	$3{\cdot}34 - 10^{-3}$	$-1{\cdot}54 \times 10^{-4}$	Present work
	−0·120	$2{\cdot}42 \times 10^{-3}$	$1{\cdot}52 \times 10^{-3}$	$-7{\cdot}76 \times 10^{-7}$	$3{\cdot}42 \times 10^{-3}$	$-1{\cdot}31 \times 10^{-4}$	Ghia *et al.*[12]
	−0·101	$2{\cdot}23 \times 10^{-3}$	$1{\cdot}93 \times 10^{-3}$	$-3{\cdot}08 \times 10^{-8}$	$5{\cdot}54 \times 10^{-3}$	$-2{\cdot}02 \times 10^{-4}$	Gresho *et al.*[13]
	−0·112	$2{\cdot}18 \times 10^{-3}$	$1{\cdot}37 \times 10^{-3}$	$-4{\cdot}07 \times 10^{-7}$	$2{\cdot}80 \times 10^{-3}$	$-6{\cdot}81 \times 10^{-5}$	Sohn[14]

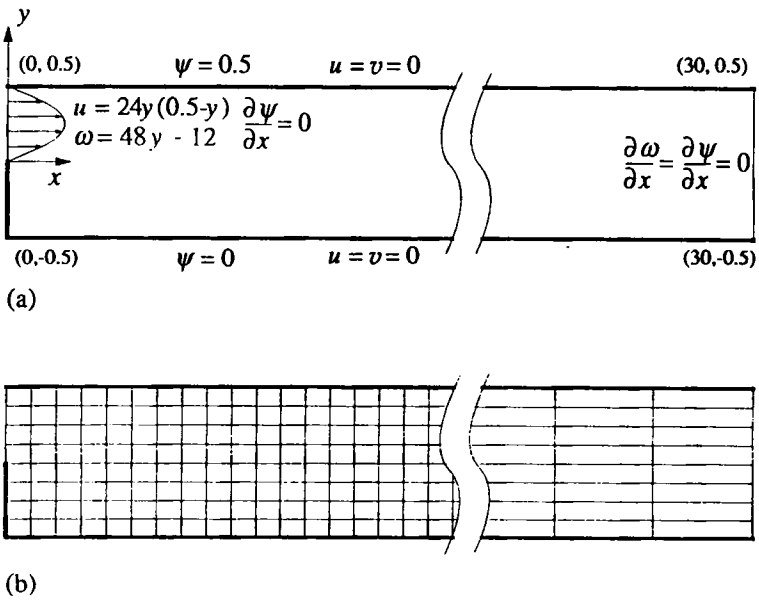

Figure 5. Two-dimensional flow over a backward-facing step: (a) geometry and boundary conditions; (b) finite element mesh

height, while the total length in the horizontal direction is 30 times the channel height. The boundary conditions include the usual no-slip velocity specification for all solid surfaces and a fully developed flow at the outlet. The inlet velocity profile corresponds to a fully developed laminar flow parallel to the channel axis, with a dimensionless parabolic, horizontal velocity component which yields an average inflow velocity $\bar{u} = 1$. The values of the vorticity at the inlet are computed by substituting the values of the velocity components into equation (9). About 2000 steps were required to reach convergence, starting from uniform initial conditions $\psi = \omega = 0$ and using a time step $\Delta t = 0{\cdot}2$.

To compare our results with the benchmark results of Gartling,[16] we assumed a value of $Re = 800$ for the Reynolds number based on the average inflow velocity and on the channel height. We used 8×120 eight-node parabolic elements (3137 grid points) with a mesh uniform across the channel. In the streamwise direction the mesh was uniformly distributed up to $x = 15$, while it was smoothly graded for $x > 15$. In this way we followed the mesh configuration illustrated in Reference 16 and we employed approximately the same number of grid points utilized for the coarsest mesh employed in that reference. In fact, Gartling[16] used five different meshes ranging from a minimum of 6×120 nine-node elements (3133 grid points) to a maximum of 40×800 elements (129,681 grid points).

The essential features of the flow are clearly illustrated by the streamfunction and vorticity contours shown in Figure 6, while the values of ψ and ω along the contours are listed in Tables IV and V respectively. The flow separates at the step edge and forms a first recirculating zone at the lower wall, while a second recirculating zone appears downstream at the upper wall. After reattachment of this upper wall eddy the flow recovers towards a full developed configuration. The results of Figure 6 compare very favourably with some of the most reliable results reported in the literature.[14,16] More quantitative comparisons regarding the two separation zones are reported in Table VI. As we can see, our results are very close to the best results of Gartling,

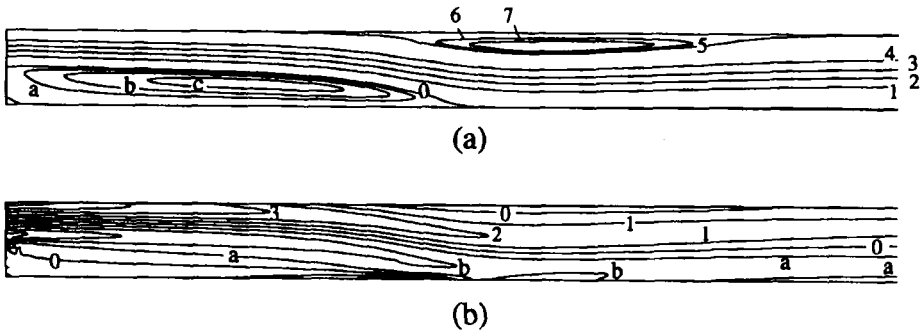

Figure 6. Laminar flow over a backward-facing step at $Re = 800$: (a) streamfunction contours (contour values are reported in Table IV); (b) vorticity contours (contour values are reported in Table V)

Table IV. Values of streamline contours in Figure 6 (a)

Contour letter	Streamfunction ψ	Contour number	Streamfunction ψ	Contour number	Streamfunction ψ
a	−0·010	0	0·000	4	0·400
b	−0·020	1	0·100	5	0·500
c	−0·030	2	0·200	6	0·502
		3	0·300	7	0·504

Table V. Values of vorticity contours in Figure 6 (b)

Contour letter	Vorticity ω	Contour number	Vorticity ω	Contour number	Vorticity ω
a	−2·0	0	0·0	3	6·0
b	−4·0	1	2·0	4	8·0
c	−6·0	2	4·0	5	10·0

obtained with a much larger number of grid points, and are certainly better than the results obtained by Gartling with his coarsest mesh.[16] Finally, in Figure 7 we compare our predictions of velocity and vorticity profiles across the channel with those of Gartling,[16] demonstrating excellent agreement. It must be pointed out, however, that our flow configuration is slightly shifted upstream and consequently the comparisons concern the same relative locations with respect to the reattachment point of the lower wall eddy (x_{RL}) and the reattachment point of the upper wall eddy (x_{RU}). Therefore our channel sections are at $x = 6{\cdot}96$ (instead of $x = 7$ as in Reference 16) and $x = 14{\cdot}96$ (instead of $x = 15$ as in Reference 14) in order to satisfy the proportions

$$x/x_{RL} = 7/6{\cdot}10 \approx 6{\cdot}96/6{\cdot}06 \approx 1{\cdot}148$$

and

$$x/x_{RU} = 15/10{\cdot}48 \approx 14{\cdot}96/10{\cdot}45 \approx 1{\cdot}431.$$

Table VI. Flow over a backward-facing step at $Re = 800$

Vortex	Centre x	Centre y	Streamfunction ψ	Vorticity ω	Separation point x_S	Reattachment point x_R	Reference
Lower wall	3·17	−0·19	−0·034	−2·34	0·00	6·06	Present work 3137 grid points
	3·00	−0·17	−0·033	−2·51	0·00	5·81	Gartling[16] 3133 grid points
	3·35	−0·20	−0·034	−2·28	0·00	6·10	Gartling[16] 129681 grid points
Upper wall	7·33	0·31	0·507	1·15	4·80	10·45	Present work 3137 grid points
	7·50	0·33	0·507	0·959	4·79	10·48	Gartling[16] 3133 grid points
	7·40	0·30	0·506	1·32	4·85	10·48	Gartling[16] 129681 grid points

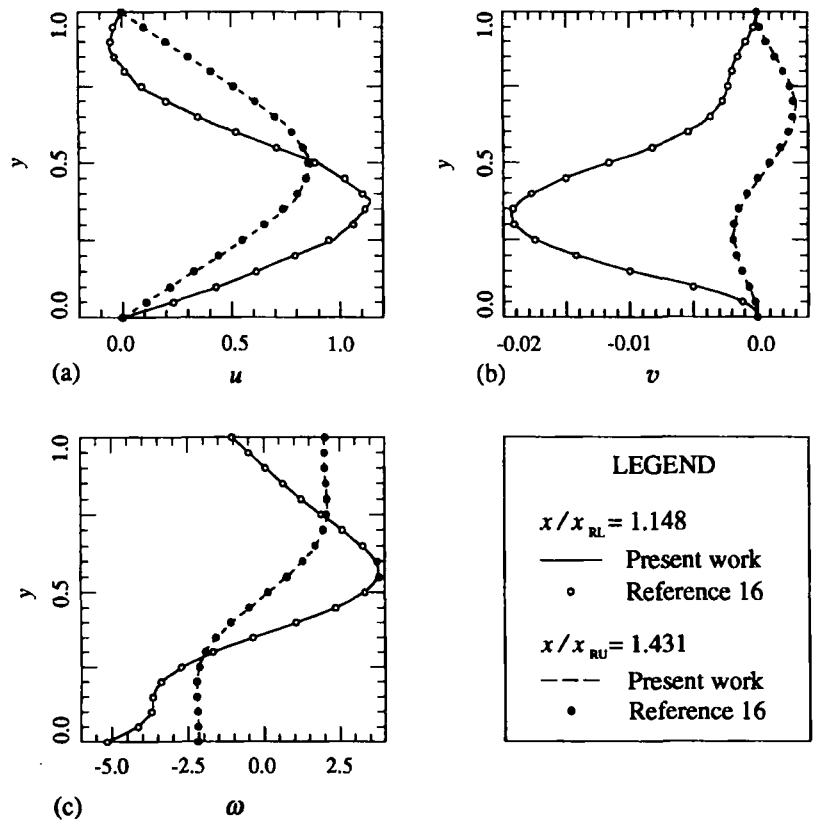

Figure 7. Laminar flow over a backward-facing step at $Re = 800$: (a) horizontal velocity profiles across the channel; (b) vertical velocity profiles across the channel; (c) vorticity profiles across the channel

5. CONCLUSIONS

The incompressible two-dimensional Navier–Stokes equations have been solved by the finite element method using a new streamfunction–vorticity formulation. The streamfunction and vorticity equations have been completely uncoupled and solved in sequence, taking advantage of a procedure that fits naturally in the framework of finite element techniques and allows an easy evaluation of vorticity at no-slip boundaries. The present scheme achieves convergence, even for very high values of the Reynolds number, without the traditional need for upwinding. Two classical benchmark problems have been solved and the results obtained have been favourably compared with some of the most accurate results available in the literature.

ACKNOWLEDGEMENTS

This research has been supported by CNR and MURST.

REFERENCES

1. P. J. Roache, *Computational Fluid Dynamics*, Hermosa, Albuquerque, NM, 1982.
2. A. Campion-Renson and M. J. Crochet, 'On the streamfunction–vorticity finite element solutions of Navier–Stokes equations', *Int. j. numer. methods eng.*, **12**, 1809–1818 (1978).
3. L. Quartapelle and M. Napolitano, 'A method for solving the factorized vorticity–stream function equations by finite elements', *Int. j. numer. methods fluids*, **4**, 109–125 (1984).
4. M. F. Peeters, W. G. Habashi and E. G. Dueck, 'Finite element stream function–vorticity solutions of the incompressible Navier–Stokes equations', *Int. j. numer. methods fluids*, **7**, 17–27 (1987).
5. T. E. Tezduyar, R. Glowinski and J. Liou, 'Petrov–Galerkin methods on multiply connected domains for the vorticity–stream function formulation of the incompressible Navier–Stokes equations', *Int. j. numer. methods fluids*, **8**, 1269–1290 (1988).
6. C. F. Kettleborough, S. R. Husain and C. Prakash, 'Solution of fluid flow problems with the vorticity–streamfunction formulation and the control-volume-based finite-element method', *Numer. Heat Transfer B*, **16**, 31–58 (1989).
7. T. E. Tezduyar, J. Liou, D. K. Ganjoo and M. Behr, 'Solution techniques for the vorticity–streamfunction formulation of two-dimensional unsteady incompressible flows', *Int. j. numer. methods fluids*, **11**, 515–539 (1990).
8. R. J. Mackinnon, G. F. Carey and P. Murray, 'A procedure for calculating vorticity boundary conditions in the stream-function–vorticity method', *Commun. Appl. Numer. Methods Eng.*, **6**, 47–48 (1990).
9. E. Barragy and G. F. Carey, 'Stream function vorticity solution using high-p element-by-element techniques', *Commun. Appl. Numer. Methods Eng.*, **9**, 387–395 (1993).
10. H. P. Langtangen, 'Conjugate gradient methods and ILU preconditioning of non-symmetric matrix systems with arbitrary sparsity patterns', *Int. j. numer. methods fluids*, **9**, 213–233 (1989).
11. V. Haroutunian, M. S. Engelman and I. Hasbani, 'Segregated finite element algorithms for the numerical solution of large-scale incompressible flow problems', *Int. j. numer. methods fluids*, **17**, 323–348 (1993).
12. U. Ghia, K. N. Ghia and C. T. Shin, 'High-*Re* solutions for incompressible flow using the Navier–Stokes equations and a multi-grid', *J. Comput. Phys.*, **48**, 387–411 (1982).
13. P. M. Gresho, S. T. Chan, R. L. Lee and C. D. Upson, 'A modified finite element method for solving the time-dependent, incompressible Navier–Stokes equations, Part 2: Applications', *Int. j. numer. methods fluids*, **4**, 619–640 (1984).
14. J. L. Sohn, 'Evaluation of FIDAP on some classical laminar and turbulent benchmarks', *Int. j. numer. methods fluids*, **8**, 1469–1490 (1988).
15. T. Tanahashi, H. Okanaga and T. Saito, 'GSMAC finite element method for unsteady incompressible Navier–Stokes equations at high Reynolds numbers', *Int. j. numer. methods fluids*, **11**, 479–499 (1990).
16. D. K. Gartling, 'A test problem for outflow boundary conditions—flow over a backward-facing step', *Int. j. numer. methods fluids*, **11**, 953–967 (1990).